TITLE   RICHTMYER-MESHKOV INSTABILITY OF SHOCKED GASEOUS INTERFACES

AUTHOR(S)   ROBERT F. BENJAMIN, M-6
DIDIER BESNARD, CEA-LIMEIL
JEAN-FRANCOIS HAAS, CEA-LIMEIL

DISCLAIMER

MASTER

RICHTMYER-MESHKOV INSTABILITY OF SHOCKED GASEOUS INTERFACES

Robert F. Benjamin
Los Alamos National Laboratory, Los Alamos, N.M. 87545, USA

Didier Besnard and Jean-François Haas, Commissariat à l'Energie Atomique
Centre d'Etudes de Limeil-Valenton, 94195 Villeneuve St-Georges Cédex, France

Abstract

The instability of shocked and reshocked perturbed interface between gases of different densities is analyzed by comparing flow visualization from 2D and 3D shock-tube experiments with 2D numerical simulations and theory. The shadowgraphs and calculations show similar large scales of mixing by fluid interpenetration induced by the Richtmyer-Meshkhov instability. In 2D, experimental instability growth following acceleration by the initial shock is less than calculated by linear theory or simulated. The 3D experiments are approximately simulated by 2D calculations with an increased initial amplitude of the interface. The kinetic energy of the interpenetrating velocity field from the simulations are also compared to a theoretical estimate derived from the linear theory.

Introduction

We performed two series of shock-tube experiments and the corresponding numerical simulations to measure effects of a pianar shock wave impulsively accelerating a perturbed interface and then decelerating it with the shock reflected from the end wall of the tube. These experiments are performed in order to explore some of the mechanisms occuring in the implosion of Inertial Confinement Fusion (ICF) targets as a consequence of Rayleigh-Taylor instabilities (RTI). In shock-tube experiments, the interface is subjected to the impulsive (i e. shock-induced) RTI, also called the Richtmyer-Meshkov instability (RMI, see Sturtevant, 1988). After the interaction with the initial shock, the interface behaviour is actually dominated by the vorticity created at shock passage by the non parallel pressure and density gradients. At the time of the reflected shock interaction, much more vorticity is created because the interface is highly distorted, in addition the preexisting vorticity is shock-enhanced. As long as the perturbation amplitude are small compared to their wavelength, the RTI or RMI are well described by a linear theory. In order to study the non-linear phase, when the amplitude to wavelength ratio is not small anymore, we rely on laboratory experiments and numerical simulations. The laboratory experiments are subjected to viscous effects acting on the shock-tube walls as well as perturbations due to the membrane initially separating the gases. The numerical simulations we use are only 2D, do not model viscous or turbulent effects and suffer from numerical dissipation. The following is a precise comparison of the growth rate of the large scales in the experiments, in the simulations and from the prediction of linear theory.

Los Alamos experiments (two-dimensional)

In this first series of experiments (Benjamin, 1988), the shape of the initial interface between gases of different densities is a 2D sine wave of wavelength λ 37.5 mm (wave number k 0.168

mm^{-1}), with a peak amplitude a of 2.4 mm. The test gas, either SF6 (sulphur hexafluoride) or helium, yielding Atwood numbers A $= \dfrac{\rho_{gas}-\rho_{air}}{\rho_{gas}+\rho_{air}}$ equal to 0.67 and -0.76, is impulsively accelerated by the Mach 1.2 planar incident shock (in air at 0.8 bar) to velocities V equal to 74 m/s and 175 m/s respectively. A 0.5 μm thick collodion membrane separates air and the test gas. The shock-tube has a cross section of 75x75 mm allowing the observation of two waves on the interface. The length of the test gas section is 92 mm hence reshock occurs early (about 1ms for air-SF6, and 0.15 ms for air-helium). The interface deformation under shock acceleration and reshock deceleration is recorded by single shot flash shadowgraphy when details are required. The reshock of the air/SF6 interface is described with the experimental shadowgraphs (fig. 1) showing the resulting shock and rarefaction waves and some mixing on the shock tube walls caused by shock-boundary layer interaction. We obtain growth rates by using multiframing shadowgraphy, giving 10 to 14 frames per shot. We find that the growth rate for air/SF6 experiments, before interaction with the reflected shock, is 16 m/s, with a 10% uncertainty and 38 m/s within 10% for air/helium experiments.

The simulations are carried out at the CEL-V using EAD, a 2D, second order, non-viscous Eulerian code. Membrane effects are not simulated; neither are turbulent boundary layers on the shock-tube walls. The interface deformation in the reshock of the air -SF6 interface are illustrated by a density and two pressure maps (fig. 2). These finely meshed numerical experiments (up to 100 cells per wavelength, and 13 in peak-to-peak amplitude) are done in order to obtain quantities such as the the thickness of the interpenetration zone (IZT, fig. 3) and the kinetic energy (IKE, fig 4) of the velocity fluctuations around the deforming interface (Besnard et. al., 1990). IZT is deduced from the y averaged mass fraction profiles: it corresponds to the region of space where the value of the mass fraction of either material lies between 0.5% and 99.5%. IKE is obtained from the local fluctuating kinetic energy calculated from the velocity components u_i :

$$\rho\, k = (\rho u_i u_i - \rho\, \hat{u}_i u_i) \quad \text{where } \rho\, \hat{u}_i = \rho\, u_i \, , \qquad (1)$$

which is then integrated along the mean flow direction (x), over the extent of the interpenetration zone, or over the total computational grid. Thus one obtains the kinetic energy (per unit area) of the fluctuating velocity field restricted to the mixing zone (ZIKE) or across the total grid, thus including also the energy due to the perturbed transmitted and reflected waves (TIKE) (fig. 4).

The growth rates from the simulations show a decrease from 26.4 m/s to 17.6 m/s in the air/SF6 case (fig. 3) and about 75 m/s in the air/helium case. The closest theoretical estimate using Richtmyer's formula,

$$\frac{dl}{dt} = \frac{4\,\pi\,a}{\lambda}\,A\,V \quad 2\,k\,a\,A\,V, \qquad (2)$$

with a being the interface amplitude after compression by the incident shock, gives 29 m/s in air/SF6 case and 78 m/s in air/helium case. We attribute the differences between the experimental and numerical values to membrane effects (diffusion and strength). The decrease observed in the air/SF6 simulation is caused by numerical dissipation and perhaps the transition into the non-linear regime.

One can also estimate from the linear analysis the amount of energy (due to velocity fluctuations) contained in the vicinity of the interface:

$$IKE = \frac{\pi a^2}{2 \lambda} V^2 A^2 (\rho_{gas} + \rho_{air}) . \qquad (3)$$

The time evolution of IKE in the simulations indicate a peak just after incident shock passage, followed by a decrease ending in a plateau. Then the reshock of the air-SF6 interface induces another, 10 times larger peak (fig. 4). In the air-helium case, the amplification due the first reshock is only 2, but the following reshocks bring the total amplification to 10. We compare peak (for incident shock) and plateau values of IKE from the simulations with Eq.(3) and find a good agreement between the theoretical estimate (corrected for compression by incident or transmitted wave) and plateau values (Besnard et. al., 1990). Equation (3), used with reshock conditions, overestimates by a factor of 4.2 the TFKE (grid) jump from the air/SF6 simulations and underestimates it by a factor of 3.1 in the air/helium case. Several other calculations performed for slightly different Mach numbers and interface amplitude and with changes in storage frequency and mesh size confirm this trend.

Caltech experiments (three-dimensional)

These experiments were performed in a square tube (cross section 89mm) with 600 mm between the initial membrane location and the end wall. The membrane (0.5 μm nitrocellulose) is mounted flat between the flanges at the junction of two test sections before being given a single 3D bulge by a small pressure difference. One or several wires can be stretched on the plane of the membrane in order to create two or more bulges. The incident shock Mach number is also 1.2 in air at 1 bar, and the gas downstream in the experiments shown here is helium, but refrigerant 22 (R22, A -0.5) or a 1/3 helium-2/3 argon mixture (A=-0.0175) were also used. The field of view extends from x=120 to x=234 mm downstream of the membrane and allows the visualization of the reflected wave interaction with the perturbed interface (at about 1 ms, figs. 5 7) but, neither the initial amplitude of the bulge(s) l_{0exp} nor the early stages of the instability can be observed. We measure instead the amplitude obtained from the quasi neutral experiments performed with the helium argon mixture, using the same conditions for setting the bulge(s), to estimate l_{0exp}: up to 20 mm (resp 10mm) for a simple (resp. twin) bulge.

The simulated 2D interface is spherical for an axisymmetric calculation or cylindrical for a planar calculation. For the single bulge, the interface shape obtained at late time with the planar calculation is in fact closer to the experimental snapshot (fig. 5) than the one obtained with the axisymmetric calculation. The initial amplitudes (L_{02D}) of the bulge in the 2D simulations are chosen such that the calculated amplitudes (L_{sim}) match the experimental ones (L_{exp}) at the lat : observation time (just before reshock, figs. 5, 6). The equivalent initial 3D bulge (L_{03D}) is obtained by multiplying L_{02D} by the ratio of the 2D (k_y) to the 3D wave number ($k = (k_y^2 + k_z^2)^{1/2}$). L_{03D} can then be compared to the value (L_{0the}) obtained by reversing the integrated version of the linear growth rate (2):

$$L_{0the} = \frac{L_{exp}}{(1 + A \ k \ V \ t)(1 - V/W_t)} \tag{4}$$

with the correction for compression by the transmitted shock of velocity W_t. In the case of the single bulge ($k = 0.1 \ mm^{-1}$), the amplitudes observed at 928 µs: $L_{exp} = 55$ mm (fig. 5) and at 1.22 ms: 75 mm $< L_{exp} < 90$ mm are obtained in a simulation with $L_{02D} = 20$ mm. This corresponds to $L_{03D} = 14.4$ mm, which is experimentally possible and about twice the theoretical value: $L_{0the} = 7.5$ mm. In the double bulge case ($k = 0.158 \ mm^{-1}$), the amplitudes at 958 µs ($35 < L_{exp} < 40$ mm, fig. 6), and at 1229 µs ($50 < L_{exp} < 75$mm, fig. 7) are simulated (fig. 8, pressure plot) with $L_{02D} = 10$ mm. This leads to $L_{03D} = 8.9$ mm (also realistic) to be compared with $L_{0the} = 2.9$ mm. This large discrepancy shows that the linear theory is clearly inadequate at this stage of the nonlinear regime of the fundamental mode. In addition, the slope discontinuities of the membrane at the wall and on the wire(s) introduce an infinite series of harmonics of the fundamental wavelength, which have also developed well into the nonlinear regime. The decrease of the growth rate of the interpenetration thickness and the evolution of IKE for the twin bulge are illustrated on figs. 9 and 10.

Conclusion

The 2D and 3D experiments and their reasonably similar 2D simulations demonstrate some aspects of the nonlinear regime of the RMI and the reshock phase. Experiments with better controlled artefacts (membrane, initial conditions) and 3D simulations should provide an improved approach.

References
Benjamin, R. (1988), Proceedings of the First International Workshop on the Physics of Compressible Turbulent Mixing (Princeton, october 1988, to be published by Springer Verlag).
Besnard D. and Haas J F. (1990), "Two dimensional simulation of contact surface instabilities in shock tube flows" 17th ISSWST, July 1989, in "Current topics in shock waves", Y. Kim ed., A I.P. Conference Proceedings 208
Sturtevant, B. (1988), "Rayleigh Taylor instability in compressible fluids", 16th ISSTW, July 1987, H Gronig ed., VCH Verlagspesellshaft, Weinheim, FRG

Figure captions

Figure 1: Shadowgraph snapshots of the SF6 (left)-air (right) interface at reshock.

Figure 2: Density map after reshock and pressure maps during reshock (SF6-air).

Figure 3: Interpenetration zone thickness (SF6-air simulation, 0.5-99.5% mass fraction).

Figure 4: Interpenetration kinetic energy in the zone and the grid (SF6-air simulation).

Figure 5: Shadowgraph snapshot of the helium (left)-air (right) single bulge before reshock.

Figure 6: Shadowgraph snapshot of the twin helium-air bulge before reshock.

Figure 7: Shadowgraph snapshot of the twin bulge after reshock.

Figure 8: Pressure maps during and after reshock (twin bulge simulation).

Figure 9: Interpenetration zone thickness (twin bulge helium-air simulation).

Figure 10: Interpenetration kinetic energy (twin bulge helium-air simulation).
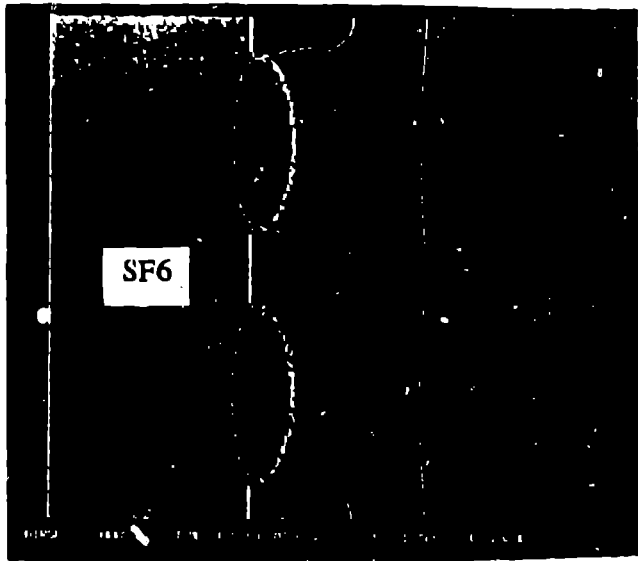
SF6

air

fig 1

SF6

air

fig 2

SF6

CM

I Z T

ERG/CM**2

TFKE

fig 3

fig 4

fig 9

fig 10

hel

fig 7

hel

fig 6

hel

air

fig 5

-4 -2 0 2 4

40
42
44
46
48
50

0.131E-07
0.135E-07
0.140E-07
0.144E-07
0.148E-07
0.152E-07
0.157E-07
0.161E-07
0.166E-07
0.170E-07

-4 -2 0 2 4

hel

40
42
44
46
48
50

air

fig 8

0.175E-07
0.179E-07
0.183E-07
0.188E-07
0.192E-07
0.196E-07
0.201E-07
0.205E-07

7